Bandgap narrowing and Mott transition in Si-doped $Al_{0.7}Ga_{0.3}N$

View Online　　Export Citation　　CrossMark

Shyam Bharadwaj,[1,a),b)] S. M. Islam,[1,b)] Kazuki Nomoto,[1] Vladimir Protasenko,[1] Alexander Chaney,[1] Huili (Grace) Xing,[1,2] (iD) and Debdeep Jena[1,2]

AFFILIATIONS

[1]School of Electrical and Computer Engineering, Cornell University, Ithaca, New York 14853, USA
[2]Department of Materials Science and Engineering, Cornell University, Ithaca, New York 14853, USA

a)Electronic mail: sb2347@cornell.edu
b)Contributions: S. Bharadwaj and S. M. Islam contributed equally to this work.

ABSTRACT

Deep ultraviolet light-emitting diodes (LEDs) composed of III-Nitride semiconductors need layers of heavy doping ($>1 \times 10^{19}$ cm^{-3}) to overcome large dopant activation energies and maintain high electrical conductivity. This work reports that at doping densities of [Si] $\sim 1.5 \times 10^{19}$/cm^3 for n-$Al_{0.7}Ga_{0.3}N$, Burstein-Moss and bandgap renormalization effects result in a net reduction of the bandgap of ~ 70 meV. At these doping levels, a transition to a metallic conductivity state is observed, with a vanishing of the effective dopant activation energy. The sheet and contact resistivities of $R_{sh,n} = 0.045$ Ω cm and $\rho_{c,n} = 1.13 \times 10^{-6}$ Ω cm^2 are achieved, with uniform conductivity in the vertical direction. The results show that when heavily doped n-AlGaN cladding regions are used for high efficiency deep-UV LEDs or lasers, the accompanying bandgap narrowing reduces the window of optical transparency at the lowest wavelengths that can take advantage of high conductivity.

Published under license by AIP Publishing. https://doi.org/10.1063/1.5086052

Deep ultraviolet (DUV) light emitting diodes (LEDs) operating at wavelengths below 260 nm (~ 4.8 eV) are of high interest for applications in sterilization and air and water purification due to high absorbance by pathogenic DNA at these wavelengths. The III-Nitride semiconductor system is ideal for such emitters due to the wide range of achievable direct bandgaps (3.4–6.2 eV).[1] Carrier injection layers for these emitters require high-Aluminum content ($>60\%$, ~ 4.87 eV) AlGaN alloys to maintain optical transparency for high-energy photon emission. However, high Al-content AlGaN layers suffer from large dopant activation energies,[2] contributing to large resistive drops, and lower wall plug efficiency (WPE) in LEDs.[3,4] It is thus necessary to increase the electrical conductivity of such electrical injection layers.

Increasing the conductivity is typically achieved by increasing the doping density to achieve a higher density of mobile carriers. As the Si substitutional donor doping density exceeds $N_D \sim 5 \times 10^{18}$/cm^3 for n-AlGaN, the Burstein Moss (BM) effect and Band Gap Renormalization (BGR) begin to have appreciable effects on the optical bandgap.[5] The BM effect occurs due to band filling in heavily doped semiconductors, resulting in an *increase* in the optical absorption edge as the Fermi level enters the band. BGR in n-type semiconductors occurs mainly due to many-particle electron-electron and electron-impurity interactions, resulting in a *decrease* in the optical gap. Determining which of these two competing effects wins in a given doping range is required to resolve the net change in the bandgap.

In this work, we demonstrate a net *reduction* in the optical bandgap of highly Si-doped (5.2×10^{18}/cm$^3 < N_D < 1.5 \times 10^{19}$/cm^3) 70% AlGaN due to a relatively weak BM effect and a strong BGR in this doping range. A transition to a metal-like conductivity state at the highest Si doping is observed, with the vanishing of the dopant activation energy. If impurity donor-doped electron injection layers similar to those studied here are used in device structures, it is crucial to take the observed bandgap reduction into account when designing LEDs to maintain high light extraction efficiency with minimal photon re-absorption.

BGR and the BM effect have been studied in many semiconductor systems including Si, GaAs, and GaN,[5–9] although whether the net effect at particular doping densities is an increase or a decrease in the optical gap has remained unclear. Indeed, in Si and GaAs, the low effective electron masses and relatively narrow bandgaps compared to AlGaN cause the two effects to occur with a similar magnitude. BGR-mediated redshifts have been observed in GaN below electron densities of 9×10^{18}/cm^3, shifting to a net BM-mediated blueshift above this density.[9] In AlN, a reduction in the bandgap due to Si-alloy formation (leading to tensile strain) has been observed with heavy Si doping despite very few free carriers (and therefore weak BM and BGR
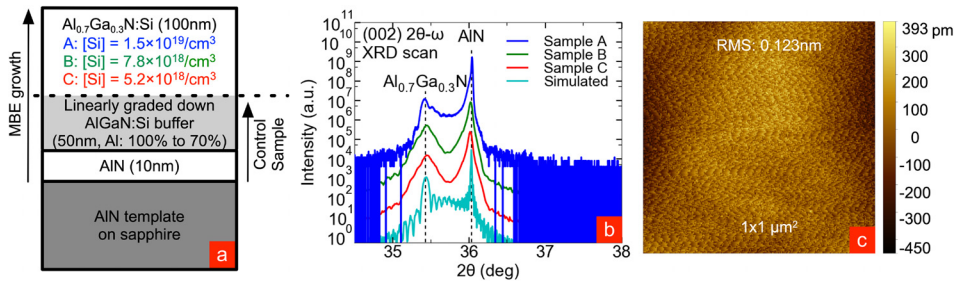
FIG. 1. (a) Structural schematic showing [Si] doping density inferred from a SIMS stack doping calibration for samples A, B, and C and the control sample consisting of just the graded buffer; (b) XRD scans for all samples (with data shifted vertically for easy comparison), showing a 70% AlGaN peak; and (c) AFM for sample B, showing the smooth surface achievable for such growths.

effects).[10,11] Bandgap reduction has not, however, been observed in heavily doped high-Al (>60%) AlGaN to date. It is theoretically predicted that the BM effect should be very weak in high-Al AlGaN due to the high conduction band effective density of states ($\sim 5 \times 10^{18}$/cm^3 for 70% AlGaN). Both electron-electron Coulomb interactions and electron-impurity interactions may contribute to BGR-mediated bandgap reduction at high electron densities, despite lack of tensile strain due to growth on smaller lattice constant AlN substrates. If electron-electron interactions are of sufficient strength, dopant based Mott transition effects should be observable. The dopant Mott transition occurs as a result of direct electron hopping conduction between orbital states centered at neighboring dopant sites, which becomes probable when the free electron density exceeds a value determined by the effective Bohr radius a_B. It is characterized by a vanishing activation energy, and the resulting electronic conductivity persists to cryogenic temperatures, as this process does not require thermal activation of electrons into the band states.

The experiments in this work aim at quantitatively elucidating the BGR, BM, and Mott transition effects in high Al-content AlGaN. To that end, three high-Al content AlGaN structures were grown in a metal-rich growth condition using plasma-assisted molecular beam epitaxy (PAMBE). As shown in Fig. 1(a), an AlN nucleation layer was first deposited on a 1 μm AlN-on-sapphire template. Then, a Si-doped AlGaN buffer layer was grown with the aluminum content graded down from 100% to 70%, followed by a 100 nm constant Si-doped 70% AlGaN transport layer. The buffer layer serves to reduce strain for the growth of the subsequent layers and simultaneously eliminate the conduction band offset that may produce unwanted charges at the abrupt heterointerface that cloud the experimental measurement of the transport properties of the subsequent doped layers. It was doped with the same level of silicon as the subsequent

transport layer, in order to compensate any polarization-induced holes. Three samples with 70% AlGaN layers of Si doping concentrations $\sim 1.5 \times 10^{19}$/cm^3 (A), $\sim 7.8 \times 10^{18}$/cm^3 (B), and $\sim 5.2 \times 10^{18}$/cm^3 (C) inferred from SIMS measurements on a doping calibration sample were grown. A separate control sample consisting only of the graded down AlGaN buffer layer on an AlN-on-sapphire substrate was grown in order to determine whether the buffer layer contributes to the transport properties of the films. This sample had an Si doping of $\sim 1.5 \times 10^{19}$/cm^3, the same as sample A, to find an upper limit to the conductivity of the graded buffers in the three samples.

Figure 1(b) shows the measured and simulated X-ray diffraction (XRD) data, confirming that the aluminum content of the top layer of all three samples is $\sim$70% and thicknesses are all $\sim$100 nm. Figure 1(c) shows the surface morphology measured by Atomic force microscopy (AFM) for sample B. Very smooth surfaces of the doped AlGaN layer with a low RMS roughness of <0.2 nm is observed, indicating high quality growth even at high Si doping concentrations. Samples A and C had RMS roughnesses of 0.448 and 0.335 nm, respectively. Maintaining a smooth surface is crucial for the subsequent growth of high-quality quantum well LED active regions.

Figure 2(a) shows the absorbance of the three samples measured by UV-Visible spectrophotometry at room temperature. The measurement was performed at normal incidence to the samples, probing transitions from the Γ_9 valence band to the conduction band (involving light with an electric field perpendicular to the c-axis or E⊥c). It is important to note that for layers with the Aluminum composition studied here, the Γ_{7+} valence band is actually closer in energy to the conduction band than the Γ_9 valence band by $\sim$150 meV, but it is only sensitive to transitions involving E∥c.[12,13] As such, the Γ_9-conduction band transition is of the highest importance rather than the
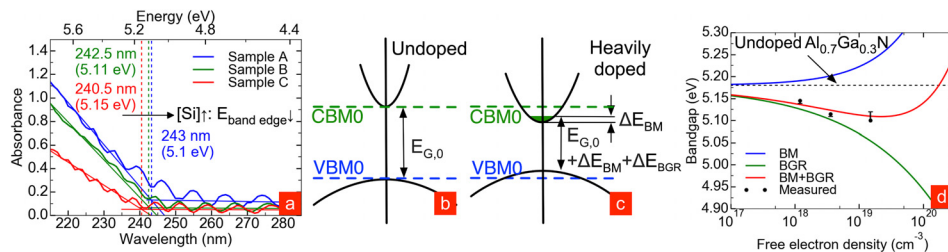

FIG. 2. (a) Absorbance profile for the 3 samples with varying silicon doping densities. As the silicon doping density goes up, the absorption band edge redshifts by 40 meV. Each sample's profile was baseline corrected to separate bare substrate pieces. (b) Schematic band structure for undoped 70% AlGaN, with no ΔE_{BM} or ΔE_{BGR}. (c) Schematic band structure for heavily doped 70% AlGaN, showing BM and BGR effects. The depicted valence band in (b) and (c) corresponds to the Γ_9 valence band. (d) Bandgap versus free electron density measured by room temperature Hall, showing a good correlation between the measured absorbance data and calculated values. The error bars are drawn to account for slight compositional and strain differences as seen in Fig. 1(b).

TABLE I. Theoretically calculated ΔE_{BM}, ΔE_{BGR}, and $\Delta E = \Delta E_{BM} + \Delta E_{BGR}$ for each of the samples in the study. Measured E_G from absorbance measurements is also displayed, along with the calculated expectation based on the experimental K coefficient (4.8×10^{-8} eV cm) from absorbance data and HSE DFT calculations for E_G (between Γ_9 and the conduction band) of undoped 70% AlGaN. The last row shows expected parameters for undoped 70% AlGaN, with calculated E_G from HSE-DFT.

Sample	[Si] (atoms/cm^3)	n_e (1/cm^3)	ΔE_{BM} (meV) Calculated	ΔE_{BGR} (meV) Calculated	$\Delta E = \Delta E_{BM} + \Delta E_{BGR}$ (meV) Calculated	E_G (eV) Calculated	E_G (eV) Measured Me
A	1.5×10^{19}	1.5×10^{19}	55	−126	−71	5.109	5.10
B	7.8×10^{18}	3.6×10^{18}	21	−79	−58	5.122	5.11
C	5.2×10^{18}	1.2×10^{18}	10	−55	−45	5.135	5.15
	0	(Intrinsic)	0	0	0	5.18	

Γ_{7+}-conduction band transition when considering layer transparency to DUV LED emission (which is predominantly E⊥c for AlGaN quantum well compositions up to ~0.8 or ~5.45 eV).[14] Fabry-Perot oscillations from the air-epi and epi-substrate interfaces are visible due to refractive index differences, with a change in the slope occurring at the onset of interband absorption. A net narrowing of the bandgap of 70% AlGaN is observed as the Si doping concentration is increased, reaching 40 meV for Si ~ 1.5×10^{19}/cm^3 compared to 5.2×10^{18}/cm^3.

The expected *increase* in the bandgap due to the BM effect ΔE_{BM} is related to the 3D free electron density n_e. For a given n_e, the Fermi wavevector is $k_F = (3\pi^2 n_e)^{1/3}$, and the Fermi energy is $E_F = \hbar 2k_F^2/2m^*$. The BM *increase* in the optical gap is thus

$$\Delta E_{BM} = +\frac{\hbar^2 (3\pi^2 n_e)^{2/3}}{2m^*}, \qquad (1)$$

where m^* is the effective mass. Contributions to ΔE_{BM} arise from both the conduction band and from the valence band since band energies at k_F are different than at the Γ point, and photons have a negligible momentum. The reduced mass is used for m^* to capture both effects. m$_e$ used in calculating the reduced mass accounts for non-parabolicity of the conduction band and degenerate doping.[15,16] ~95% of the contribution to ΔE_{BM} arises from the conduction band due to its relatively low effective mass (m$_e < 0.4$m$_0$ for 70% AlGaN), as compared to the much larger Γ_9 valence band effective mass (m$_{hh,\perp} \sim 5$m$_0$ for 70% AlGaN).[17]

On the other hand, the *decrease* in the bandgap due to many-particle renormalization effects can be modeled as

$$\Delta E_{BGR} = -K n_e^{1/3}, \qquad (2)$$

with

$$K = f \frac{q^2}{4\pi\epsilon}, \qquad (3)$$

where K is related to the overlap of ionized donor Coulomb potentials, q is the electron charge, ϵ is the dielectric constant, and f is a geometric factor related to the probability of finding an ionized donor near another ionized donor, equal to $\Gamma(2/3)(4\pi/3)^{1/3}$.[18,19] Figures 2(b) and 2(c) illustrate the contributions of these two effects on the optical bandgap for undoped and heavily doped AlGaN. The experimentally reported values of K range from ~2.6 to 5.8×10^{-8} eV cm in GaN,[5,8,20] showing agreement with the calculated value of ~3.5×10^{-8} eV cm using Eq. (3). Figure 2(d) shows that the fit to the measured absorption band edges vs n_e (measured by room temperature Hall using van-der-Pauw geometry) for 70% AlGaN requires K ~ 4.8×10^{-8} eV cm. In all cases, the contacts were ohmic. The calculated values for ΔE_{BM}, ΔE_{BGR}, ΔE, and E_G using

this K are shown in Table I. Undoped 70% AlGaN is forecasted to have a bandgap of ~5.18 eV, consistent with theoretical HSE (Heyd-Scuseria-Ernzerhof) DFT (Density Functional Theory) calculations[21,22] and others' experimental results.[12,13] This experimental K is slightly higher than the calculated value of ~3.7×10^{-8} eV cm from Eq. (3). Slight differences in the strain and Al content (<0.8%) in the three samples may contribute to the increased experimental K value—error bars are drawn in Fig. 2(d) as upper and lower bounds of measured gap due to these effects. It is important to note that the qualitative dependence of bandgap on free electron density does not change using the smaller calculated K value: still, at $n_e = 1.5 \times 10^{19}$/cm^3, a net *redshift* of ~40 meV is expected from using the calculated K from Eq. (2) rather than the experimental one. Nonetheless, the experimental K shows consistency with the observed activation energies from temperature dependent Hall-effect transport measurements shown in Fig. 3(a) and the carrier density required for the vanishing of donor activation energy, as shown in the following analysis.
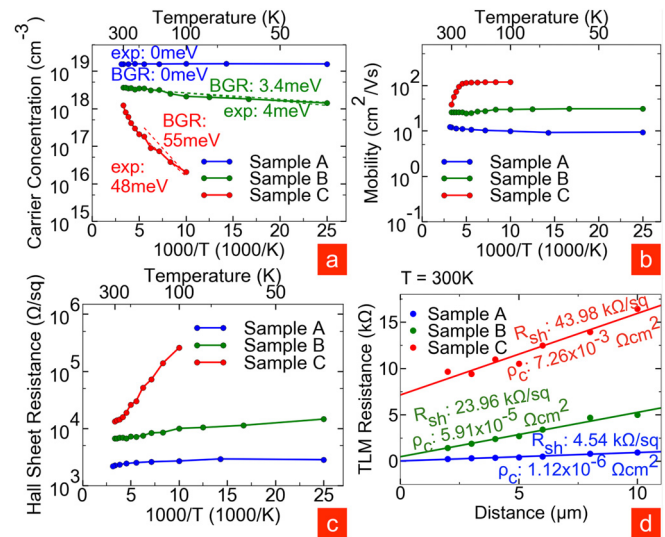

FIG. 3. (a), (b), and (c) Temperature-dependent Hall measurements for the three samples. As the silicon doping density rises, activation energy falls. The volumetric free carrier concentration in (a) is determined by dividing the measured sheet density by layer thickness estimated from XRD. The calculated experimental activation energy (exp) is shown along with theoretical activation energies (BGRs). The carrier concentration is shown in (a), mobility in (b), and sheet resistance in (c). (d) TLM measurements for the three samples, showing the increasing sheet and contact resistance with the decreased doping level.

The observed activation energies and carrier density required for vanishing activation energy should satisfy the following relation according to the BGR theory:[19]

$$E_D = E_D(N_{Si,+} = 0) - K N_{Si,+}^{1/3}, \qquad (4)$$

where E_D is the donor activation energy, $N_{Si,+}$ is the density of ionized donors, and $E_D(N_{Si,+} = 0)$ is the donor activation energy in the case of very few donors. Using the experimental K value obtained earlier, activation energies from Eq. (4) match well with experimentally measured values if $E_D(N_{Si,+} = 0) = 77$ meV is used. This $E_D(N_{Si,+} = 0)$ value is reasonably consistent with the effective mass theory value (50–60 meV) for shallow Si donors in 70% AlGaN[23,24] and with experimental Hall results for lightly Si doped AlGaN of similar Al mole fraction,[2] suggesting that Si behaves as a shallow donor at these aluminum concentrations. It is predicted that DX center formation will only occur at higher aluminum compositions.[25] Measured activation energies were determined using a simple two-level activation model

$$n(T) \propto e^{-E_D/kT}, \qquad (5)$$

where k is the Boltzmann constant and T is the temperature in Kelvin. Calculated versus measured values are shown alongside dashed linear fits in Fig. 3(a).

Using $E_D(N_{Si,+} = 0) = 77$ meV, Eq. (4) predicts the vanishing of activation energy ($E_D = 0$) at $N_{Si,+} \sim 3.1 \times 10^{18}$/cm³. Mott theory separately provides a method for calculating $n_e = N_{Si,+}$ at which the activation energy should vanish. A Mott transition is expected to occur at $n_e = N_{Mott} = (C/a_B)^3$,[3] with C values reported between 0.2 and 0.25,[26,27] and the effective Bohr radius of donors in semiconductors, $a_B = a_H$ (ϵ/m^*), is equal to 1.3×10^{-7} cm for Si donors in 70% AlGaN. The magnitude of C is determined by satisfying the condition that no bound states exist for the 3D Coulomb potential between carriers and ionized dopants and produces a range for $N_{Mott} \sim 3.3–6.5 \times 10^{18}$/cm³ for 70% AlGaN, showing excellent agreement between Mott theory, BGR theory, and the experimental measurement. While the Mott effect has been observed in 70% AlGaN by others,[24] it has been seen at much higher free electron concentrations $>3 \times 10^{19}$/cm³ and with activation energies still >2 meV. Our results show the transition occurring at predicted values with the complete vanishing of the activation energy in heavily n-doped AlGaN.

The Arrhenius plots in Fig. 3(a) indicate a clear trend: the effective activation energy E_D falls sharply with an increase in the Si doping concentration. The conductivity transitions from a metallic state with zero activation energy at a free electron density between $n_e \sim 3.6 \times 10^{18}$/cm³ and 1.5×10^{19}/cm³ to a doped semiconducting state at lower doping densities. This transition is consistent with the observed trends in mobility and sheet resistance [Figs. 3(b) and 3(c)]: at the lower doping densities, mobility reaches higher values (~ 120 cm²/Vs) at low temperatures, indicating that ionized impurity scattering is weaker in these samples. At high doping levels, Mott conduction strongly reduces the temperature dependence of transport, so mobility stays relatively constant. The sheet resistance of the more lightly doped samples increases as expected with decreasing temperature, with the overall sheet resistance decreasing with increased doping density. Despite reduced mobility for the most heavily doped samples, the sheet resistance from transfer length method (TLM) measurements [Fig. 3(d)] decreases for heavier doping.

The validity of these Hall and TLM measurements on the samples in this study relies on the Si doped graded AlGaN buffer being insulating. Polarization-induced doping should result in $\sim 3 \times 10^{18}$/cm³ holes based on the layer thickness and range of compositions graded between, while the impurity-based doping may result in a similar number of free electrons if activation energies are high for AlGaN with an Al mole fraction $>80\%$. Upon the measurement, this control sample in which the polarization field opposed the ionization of Si dopants was found to be highly resistive (>10 MΩ/sq). This confirmed that the buffer graded AlGaN layer in Fig. 1(a) does not contribute to the electrical conductivity in the TLM patterns nor in the Hall-effect measurement. From the TLM measurements on sample A [Fig. 3(d)], a contact resistivity of $\rho_{c,n} = 1.13 \times 10^{-6}$ Ω cm² and a sheet resistivity of $R_{sh,n} = 0.045$ Ω cm are measured, suggesting excellent lateral conductivity, on par with the best results reported earlier, albeit for much thicker layers.[28–30] The current spreading length in a mesa geometry p-n junction LED with low specific contact resistances is $L_S = (nkTt_n/q\rho_n J_0)^{1/2}$, where n is the ideality factor, k is the Boltzmann constant, T is the temperature, t_n is the layer thickness, ρ_n is the layer resistivity, and J_0 is the current density.[30] Using $n = 5$, $J_0 = 10$ A/cm², and the measured n-layer resistivity produces $L_S = 17$ μm but rises to 54 μm for $t_n = 1$ μm. Thus, the use of a thick n-layer with conductivity as in sample A will be suitable for high performance UV LEDs.

In performing the transport and BGR analysis above, we have assumed that the Si distribution, and thus the electron density, is uniform throughout the AlGaN layers in the vertical direction. If there is significant nonuniformity, degenerate accumulation layers or 2D electron gases may form due to band offsets and quantum confinement. To probe vertical transport properties and ensure that no such layers are the reason for vanishing activation energy from the Hall effect, we employed a controlled inductively coupled plasma reactive ion etching (ICP-RIE) etch series, followed by Hall-effect measurements to determine the differential resistivity of individual cross-sectional wedges of the most heavily doped AlGaN layer (sample A). The etch depths were determined by stylus profilometry. The results of this series of Hall-effect measurements are tabulated in Table II, and the extracted resistivity vs depth is plotted in Fig. 4. The extracted resistivity of each individual wedge is marked at a point in the center of the wedge in Fig. 4. The resistivity is found to be quite uniform with the depth, and the extracted mobility is constant, indicating that the electron distribution is uniform, and no two-dimensional electron gases or accumulation layers exist. This corroborates our claim that the lack of freezeout in the temperature-dependent Hall measurement stems from the formation of an impurity band and not the formation of a parasitic 2DEG.

TABLE II. Hall data for the sample with [Si] = 1.5×10^{19}/cm³, showing the carrier concentration, mobility, and sheet resistance as a function of the etch depth. Repeated measurements produce mobility values within 1 cm²/Vs of listed values.

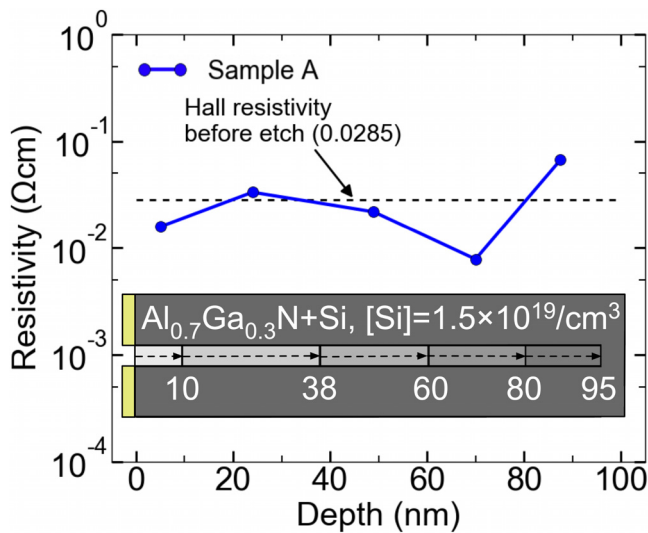| Etch depth (nm)	Carrier conc. (cm⁻³)	Mobility (cm²/Vs)	R_{sh} (kΩ/sq) Calculated
0	1.474×10^{19}	14.9	1.90
10	1.505×10^{19}	13.7	2.16
38	1.535×10^{19}	14.4	2.64
60	1.501×10^{19}	12.4	3.6
80	1.502×10^{19}	6.21	44.5
95	…	…	$>1 \times 10^4$

FIG. 4. Extracted resistivity profile versus depth, treating each etched wedge as part of a network of parallel resistors that make up the whole layer (the device cross-section is shown in the inset). Resistivity is relatively uniform in the sample, indicating uniform vertical electron distribution.

In conclusion, we quantitatively elucidate the phenomenon of bandgap narrowing in heavily Si-doped 70% AlGaN and observe a Mott transition to metallic conductivity at a relatively low free carrier density between $n = 3.6$ and $1.5 \times 10^{19}/\text{cm}^3$. A net $\sim$70 meV redshift of optical bandgap is measured for $n_e = 1.5 \times 10^{19}/\text{cm}^3$ due to a stronger BGR effect than the BM effect stemming from a high $K \sim 4.8 \times 10^{-8}$ eV cm. The resistivity measured by the Hall-effect in samples beyond the Mott transition is low (0.0285 Ω cm), and the free electron distribution is vertically uniform, making such layers suitable for electron injection layers in UV LEDs. The surface morphology is sufficiently smooth for the active region and subsequent p-cladding growth. A further study of intermediate and higher Si doping densities will help to illuminate the BGR trend with more accuracy. As long as the crystal quality is not compromised, doping n-layers as heavily as possible is ideal for optical device performance (due to increased charge by $\sim$10$\times$ and decreased mobility by only $\sim$2$\times$ in the doping range studied), so long as the energy gap narrowing is taken into account to ensure optical transparency. The study presented here should also be useful for AlGaN channel high-voltage field-effect transistors by offering guidelines in the tradeoff between mobility, free carrier concentration, and conductivity. Since in the nitride heterostructures, one can introduce free carriers in the bands *without* impurities by taking advantage of polarization-induced doping,[31,32] an interesting scientific question for the future is to explore how the bandgap renormalization and Burstein-Moss shifts observed here for impurity doped samples play out for such unconventional layers.

REFERENCES

[1]S. Nakamura, "Gallium nitride I," in *Semiconductors and Semimetals*, edited by J. I. Pankove and T. D. Moustakas (Academic, New York, 1998), Vol. 50, pp. 431–457.

[2]A. Y. Polyakov, N. B. Smirnov, A. V. Govorkov, M. G. Milvidskii, J. M. Redwing, M. Shin, M. Skowronski, D. W. Greve, and R. G. Wilson, Solid-State Electron. **42**, 627 (1998).

[3]A. Khan, K. Balakrishnan, and T. Katona, Nat. Photonics **2**, 77 (2008).

[4]H. Hirayama, Y. Tsukada, T. Maeda, and N. Kamata, Appl. Phys. Express **3**, 031002 (2010).

[5]M. Yoshikawa, M. Kunzer, J. Wagner, H. Obloh, P. Schlotter, R. Schmidt, N. Herres, and U. Kaufmann, J. Appl. Phys. **84**, 4400 (1999).

[6]S. Mohammad and M. Sobhan, Phys. Status Solidi B **156**, 287 (1989).

[7]C. Spataru, L. Benedict, and S. Louie, Phys. Rev. B **69**, 205204 (2004).

[8]H. Schenk, S. Borenstain, A. Berezin, A. Schön, E. Cheifetz, S. Khatsevich, and D. Rich, J. Appl. Phys. **103**, 103502 (2008).

[9]M. Feneberg, S. Osterburg, K. Lange, C. Lidig, B. Garke, and R. Goldhahn, Phys. Rev. B **90**, 075203 (2014).

[10]E. Monroy, J. Zenneck, G. Cherkashinin, O. Ambacher, M. Hermann, M. Stutzmann, and M. Eickhoff, Appl. Phys. Lett. **88**, 071906 (2006).

[11]K. Nam, M. Nakarmi, J. Li, J. Lin, and H. Jiang, Appl. Phys. Lett. **83**, 2787 (2003).

[12]M. Feneberg, M. Winkler, J. Klamser, J. Stellmach, M. Frentrup, S. Ploch, F. Mehnke, T. Wernicke, M. Kneissl, and R. Goldhahn, Appl. Phys. Lett. **106**, 182102 (2015).

[13]B. Neuschl, J. Helbing, M. Knab, H. Lauer, M. Madel, K. Thonke, T. Meisch, K. Forghani, F. Scholz, and M. Feneberg, J. Appl. Phys. **116**, 113506 (2014).

[14]R. G. Banal, M. Funato, and Y. Kawakami, Phys. Rev. B **79**, 121308 (2009).

[15]D. Cavalcoli, S. Pandey, B. Fraboni, and A. Cavallini, Appl. Phys. Lett. **98**, 142111 (2011).

[16]M. Bouzidi, Z. Benzarti, I. Halidou, S. Soltani, Z. Chine, and B. EL Jani, Mater. Sci. Semicond. Process. **42**, 273 (2016).

[17]L. Cláudio de Carvalho, A. Schleife, and F. Bechstedt, Phys. Rev. B **84**, 195105 (2011).

[18]K. F. Berggren and B. E. Sernelius, Phys. Rev. B **24**, 1971 (1981).

[19]W. Götz, R. S. Kern, C. H. Chen, H. Liu, D. A. Steigerwald, and R. M. Fletcher, Mater. Sci. Eng. B **59**, 211–217 (1999).

[20]G. Zhou, G. Yu, T. Egawa, J. Watanabe, T. Jimbo, and M. Umeno, Appl. Phys. Lett. **71**, 2424 (1997).

[21]J. L. Lyons, A. Janotti, and C. G. Van de Walle, Phys. Rev. B **89**, 035204 (2014).

[22]S. R. Lee, A. F. Wright, M. H. Crawford, G. A. Petersen, J. Han, and R. M. Biefeld, Appl. Phys. Lett. **74**, 3344 (1999).

[23]X. Thang Trinh, D. Nilsson, I. G. Ivanov, E. Janzén, A. Kakanakova-Georgieva, and N. Tien Son, Appl. Phys. Lett. **105**, 162106 (2014).

[24]K. Zhu, M. Nakarmi, K. Kim, and H. Jiang, Appl. Phys. Lett. **85**, 4669 (2004).

[25]L. Gordon, J. L. Lyons, A. Janotti, and C. G. Van de Walle, Phys. Rev. B **89**, 085204 (2014).

[26]N. Mott, Rev. Mod. Phys. **40**, 677 (1968).

[27]A. Ferreira da Silva and C. Persson, J. Appl. Phys. **92**, 2550 (2002).

[28]R. France, T. Xu, P. Chen, R. Chandrasekaran, and T. Moustakas, Appl. Phys. Lett. **90**, 062115 (2007).

[29]T. Al tahtamouni, J. Lin, and H. Jiang, J. Appl. Phys. **113**, 123501 (2013).

[30]H. Kim, J. Cho, J. Wook Lee, S. Yoon, H. Kim, C. Sone, Y. Park, and T. Seong, IEEE J. Quantum Electron. **43**, 625 (2007).

[31]D. Jena, S. Heikman, D. Green, D. Buttari, R. Coffie, H. Xing, S. Keller, S. DenBaars, J. Speck, and U. Mishra, Appl. Phys. Lett. **81**(23), 4395 (2002).

[32]J. Simon, V. Protasenko, C. Lian, H. Xing, and D. Jena, Science **327**(5961), 60 (2010).